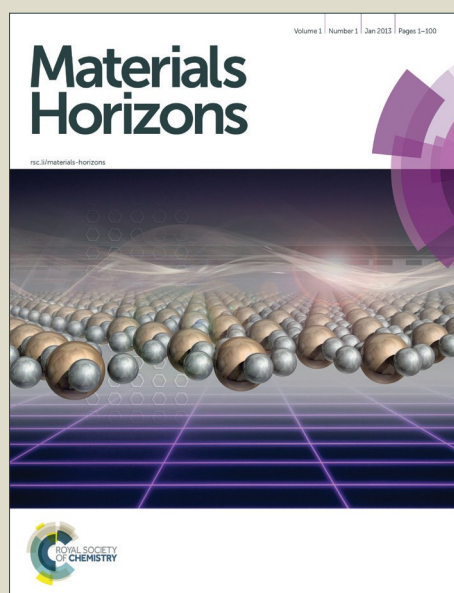


# Materials Horizons

Accepted Manuscript



This is an *Accepted Manuscript*, which has been through the Royal Society of Chemistry peer review process and has been accepted for publication.

*Accepted Manuscripts* are published online shortly after acceptance, before technical editing, formatting and proof reading. Using this free service, authors can make their results available to the community, in citable form, before we publish the edited article. We will replace this *Accepted Manuscript* with the edited and formatted *Advance Article* as soon as it is available.

You can find more information about *Accepted Manuscripts* in the [Information for Authors](#).

Please note that technical editing may introduce minor changes to the text and/or graphics, which may alter content. The journal's standard [Terms & Conditions](#) and the [Ethical guidelines](#) still apply. In no event shall the Royal Society of Chemistry be held responsible for any errors or omissions in this *Accepted Manuscript* or any consequences arising from the use of any information it contains.

# Vivid Colorful Hybrid Perovskite Solar Cells by Doctor-Blade Coating with Perovskite Photonic Nanostructures

*Yehao Deng, Qi Wang, Yongbo Yuan and Jinsong Huang<sup>\*1</sup>*

Department of Mechanical and Materials Engineering, University of Nebraska-Lincoln, Lincoln, Nebraska 68588-0656, USA.

**Key words:** Perovskite; solar cells; concentric rings; photonic crystals

**Conceptual insights:** Solar cell is a promising technology to replace fossil fuel and become one of the major energy sources globally. Among several advantageous form factors, the color of the organic and hybrid solar cells has important impact in their adoption by customer for the niche applications such as building-integrated photovoltaics (BIPV) and portable chargers. The color and semi-transparency of these solar cells add values of decoration to these third generation solar cells in addition to the energy generated. The pioneering work in colorful perovskite solar cells by *Snaith* and co-workers (*Nano Lett.*, 2015, 15 (3), pp 1698–1702) inherited the concept of organic solar cells in which the color was achieved by the incomplete absorption of the visible light. Here we presented a completely new mechanism to achieve vivid colorful solar cells using the spontaneously generated photonics nanostructure during the doctor-blade coating, which is a scalable fabrication process for large area colorful solar cell manufacturing. These colorful solar cells are also surprisingly efficient. Our analysis shows that only perovskite based colourful

---

<sup>1</sup> \*Correspondence should go to J. Huang at [jhuang2@unl.edu](mailto:jhuang2@unl.edu)

solar cells may have high efficiency due to their unique defect physics, although such photonic structures may form in different material systems.

**Abstract:** The colors of solar cells are very important in adopting them for future in-door and out-door light energy harvesting with smart designs. Here we report the formation of vivid colorful hybrid organometal trihalide perovskite solar cells by a low-cost and scalable doctor-blade coating method. The perovskite films have a combination of hundred micrometer size large domain structure and concentric ring photonics structure in each domain which generates the vivid color. The convection during precursor solution drying in doctor-blade coating process has been found to be responsible for the formation of large domain and coffee-ring like perovskite photonic structures after solvent drying, whose periodicity can be well tuned by substrate temperature and precursor solution concentration. Both the perovskite films and the finished devices are very colorful, and the efficiency of the vivid colorful solar cells is close to the optimized perovskite solar cells by doctor-blade coating.

### **Main text**

As one most important “selling points” of organic solar cells, the unique tunable colors of organic solar cells are recognized as important as their power conversion efficiency (PCE) for the building integrated photovoltaics (BIPV) applications.<sup>1</sup> The most efficient solar cells are always black in order to absorb as more light as possible, but colorful solar cells can not only provide electricity for our daily need, but also act as a decoration to our living surroundings, including clothing, vehicles and buildings.<sup>2,3</sup> Though colorful solar cells have relatively lower

PCE because they allow some spectrum of visible light to pass through and/or be reflected to have colorful appearance, there have been sustaining endeavors in fabricating colorful solar cells, particularly those made of semiconducting polymers.<sup>4-11</sup> However, there are still issues with the many reported colorful solar cells that limit their application potential. First, the fabrication cost and time would increase a lot because the one or two dimensional photonic structures for color appearance are often processed by expensive and time-consuming high vacuum thermal evaporation or lithography.<sup>5, 12, 13</sup> Second, the PCE of colorful solar cells are generally well below that of their regular black counterparts because of the much thinner photoactive layer for the see-through mode devices or increased device resistance and/or carrier recombination by complicated photonic structure.<sup>9, 11</sup> Here, we report a new type of colorful solar cell based on organometal trihalide perovskite (OTP) materials formed by a low cost doctor-blading method, which could reverse the above-mentioned disadvantages. The two dimensional photonic structures on the OTP films form spontaneously and instantly by Rayleigh–Bénard convection<sup>14-18</sup> and “coffee ring” effect<sup>19-24</sup> during doctor-blade coating within 1-2 seconds in ambient condition. The solar cell based on such OTP film has a stabilized PCE of 12.2%, maintaining 80% of the efficiency of standard black OTP solar cells fabricated in a similar way.<sup>25</sup> The high PCE despite complex photonic structure is ascribed to the superior carrier transportation and defect physics nature of OTP materials.

The process of OTP film formation by doctor-blade coating is shown in Figure 1a. A substrate (e. g. hole transport layer coated indium tin oxide (ITO) on glass) was kept at 100 ~ 160 °C on a hotplate. A drop of  $\text{CH}_3\text{NH}_3\text{PbI}_3$  ( $\text{MAPbI}_3$ ) dissolved in *N, N*-dimethylformamide (DMF) solution was swiped linearly by a glass blade quickly (0.75 mm/s) to form a thin wet film on the substrate. As solvent evaporated,  $\text{MAPbI}_3$  crystals nucleated grow in size and drift along with the

solvent convection driven by the temperature difference  $\Delta T$  between the bottom and top surfaces of the thin layer of solution (Rayleigh–Bénard convection).<sup>14</sup> Due to the high substrate temperature, the film dried within 1~2 seconds and left a MAPbI<sub>3</sub> polycrystalline film finally. We found that when the solution concentration was below a certain value (~350 mg/ml), a vividly colorful OTP film was obtained, as is shown in Figure 1c. The left image is an as-prepared OTP film, and the right image is a complete solar cell device with thermal evaporated aluminum electrode on the top. Both photos were taken in reflection mode from the film side. The microstructure of an as-prepared film is shown in Figure 1b and D by scanning electron microscopy (SEM) from cross section and top view, respectively. The films are composed of two kinds of regular patterns on different length scale: polygon domains (highlighted by purple) on the scale of 20-100  $\mu\text{m}$  with size depending on the substrate temperature, and a series of concentric rings (highlighted by red) with a thickness of ~350 nm and a nearly equal ring to ring spacing in each domain. The ring space is between 2  $\mu\text{m}$  and 6  $\mu\text{m}$  depending on the solution concentration. Higher magnification cross section SEM in the upper panel in Figure 1b shows that each ring is composed of many MAPbI<sub>3</sub> nanocrystals with an average size of around 500 nm. We found that the concentric ring structures always accompany with the vivid color of the films. The low concentration of the MAPbI<sub>3</sub> precursor solution is critical in yielding the formation of the concentric rings by the doctor-blade coating. When the MAPbI<sub>3</sub> precursor solution concentration was increased to above 350 mg/ml, the concentric rings disappeared, but only polygon domains left in the film (Figure S1 a). The bladed films were black without the perovskite photonic structure, agreeing with our previous study.<sup>25</sup> This highly periodic concentric ring structure on micrometer scale works as a reflection grating in the visible light range, which splits and diffracts the reflected visible light into different directions, depending on

the wavelength. The selective reflection results in a vivid colorful appearance in the whole visible light spectrum for the doctor-bladed OTP films. It is noted that similar structural color is also observed in CD/DVD disks or regular optical gratings, which contain small trenches on the micrometer/sub-micrometer scale and also interact with visible light vividly.

Such spontaneous formation of the photonic structures in the OTP films is scalable to large area colorful solar cells fabrication. It is then highly interesting to learn how such patterns form and evolve. First of all, the polygon domains squeezing with each other resemble the classic Bénard cell pattern by Rayleigh–Bénard convection.<sup>15,18</sup> As illustrated in Figure 1a, the solution close to the substrate with higher temperature tends to flow upward by the Buoyance force due to its relatively lower density than the surrounding colder solution.<sup>18</sup> When the hot solution reaches the top surface, its temperature decreases and it flows back to the bottom to get heated again. A number of localized convections form in this way within the thin solution films. Each convection cell tends to push each other in surrounding due to their reverse circulation direction at the edge of the cell, forming polygon patterns as illustrated in Figure 2a. The OTP material in the solution is driven by the convection, and thus inherits the polygon patterns, resulting in polygon pattern in the solid films after drying. Since the convection is driven by the temperature gradient ( $\Delta T$ ), changing the substrate temperature can modify the convection flow strength, and thereby changes the polygon domain size. As is shown in Figure 2b-d, when the substrate temperature increased from 100 °C to 160 °C the domain size increased from 20  $\mu\text{m}$  to over 100  $\mu\text{m}$ . This can be explained by the longer range convection under a higher temperature gradient. The similar pattern reported very recently by *W. Nie et. al*<sup>26</sup> can also be explained by the convection because of the heated ITO substrate used in that study. In the as-prepared OTP films,

the Bénard cells showed up from 130 °C on with size of  $\sim 30 \mu\text{m}$  and increases to  $\sim 200 \mu\text{m}$  when temperature was increased to 190 °C.<sup>26</sup>

The concentric ring photonic structure within each domain can be explained by another convection mechanism of “coffee ring effect”.<sup>19, 20, 22-24</sup> Typically, coffee ring effect occurs when a drop of solution containing nonvolatile solutes is drying on a solid surface.<sup>19</sup> Normally the contact line between the edge of the solution droplet and the solid surface is pinned on the surface, thus during drying, solution in the interior keeps flowing to the contact line region to replenish the solvent evaporated there in order to prevent the contact line from contracting.<sup>19, 23</sup> The solutes are carried along with the outward flow to the contact line, which results in the formation a dense ring at the contact line after drying.<sup>19, 23</sup> In many cases, the contact line of a droplet contracts toward the interior in a manner of alternative pinning and de-pinning process during the solvent evaporation due to the competition between the pinning force (tends to fix the contact line) and the surface tension of solution (tends to induce droplet shrinkage and thus contract the contact line).<sup>20, 21</sup> During the pinning period, as solvent is flowing to the contact line and evaporating, the solution flattens out and then the contact angle on the contact line decreases. Decreased contact angle increases the lateral component of surface tension of solution, which eventually balances the pinning force, then the contact line starts to move inward to release the lateral surface tension by shrinking the droplet to increase the contact angle, i.e. de-pinning. Once the lateral surface tension is released, the contact line is pinned again. During this pinning and de-pinning process, the solutes (OTP material and nanocrystals in this case) piles up along every contact line during every pinning period, forming a series of narrow concentric rings instead of one wide ring after drying, as is illustrated by the cross section view in Figure 3a.<sup>22, 24</sup> To find out whether the concentric ring structure in the OTP films formed in the same manner, we

“freeze” the films at different stages during drying by dropping toluene as the anti-solvent to extract the solvent *N,N*-dimethylformamide (DMF) in a very short time. Toluene can mix with DMF but can't dissolve OTP material, thus a drop of toluene can quickly remove DMF from the solution and prevent the film's microstructure from further evolving.<sup>27,28</sup> The corresponding top view SEM images at different stage of film evolution are shown in Figure 3b. It is consistent with above description that the rings appeared first from the edge, and then gradually developed inward to the center of the domain. Therefore, it is concluded that the concentric rings structure causing the vivid color of the OTP films is formed by the “coffee-ring effect”. We found that by decreasing the solution concentration from 350 mg/ml to 180 mg/ml the ring spacing decreased from 6  $\mu\text{m}$  to 2  $\mu\text{m}$  (Figure S1 b and c), giving the flexibility in tuning the periodicity of the spontaneous photonic structures in the OTP films and thus their color. It can be explained by the difference of time that needs to reach the supersaturated condition for the  $\text{MAPbI}_3$  nanocrystal formation. The nanocrystals can form by nucleation of  $\text{MAPbI}_3$  at the solution surface which provide a heterogeneous interface of easy nucleation. Since the space of the substrate the slide glass is fixed, a lower precursor solution concentration leads to a thinner solution film when  $\text{MAPbI}_3$  crystals start to nucleate, because it needs to evaporate more solvent to reach the same supersaturation point. A thinner film experiences a faster increase of lateral surface tension due to the smaller contact angle on the contact line. Therefore, the critical point when pinning force and lateral surface tension are balanced occurs more frequently, thus the pinning/de-pinning frequency increases, the ring spacing decreases for the films drying from the less  $\text{MAPbI}_3$  concentration. It is noted that the whole processes were finished in  $\text{N}_2$  glovebox, and thus the influence of moisture to the photonic structure was not studied here, but it can be an interest topic for followed up study.

The vivid colorful OTP solar cells have a device structure of ITO/Poly[bis(4-phenyl)(2,4,6-trimethylphenyl)amine] (PTAA)/CH<sub>3</sub>NH<sub>3</sub>PbI<sub>3</sub>/[6,6]-phenyl-C61-butyric acid methyl ester (PC<sub>60</sub>BM)/C60/2,9-dimethyl-4,7-diphenyl-1,10-phenanthroline (BCP)/Aluminum, as shown in Figure 4a.<sup>29-32</sup> Under simulated one sun light illumination (100 mW/cm<sup>2</sup>), the device had a short circuit current ( $J_{sc}$ ) of 18.9 mA/cm<sup>2</sup>, an open circuit voltage ( $V_{oc}$ ) of 0.89 V and a fill factor ( $FF$ ) of 72% (Figure 4b). The moderately reduced  $J_{sc}$  and  $V_{oc}$  comparing to the optimized black OTP device fabricated by the doctor-blade coating with  $J_{sc}$  of 21.8 mA/cm<sup>2</sup> and  $V_{oc}$  of 1.05 V<sup>25</sup> can be explained by the smaller grain size and thus higher grain boundary density in the colorful films that increases charge recombination rate.<sup>33</sup> The grain growth during the annealing process is spatially limited by the width of each ring, otherwise the grains can grow into several micrometers.<sup>29</sup> The external quantum efficiencies (EQEs) shown in Figure 4c were measured by tilting the angles between the incident light and the normal direction of the device plane from 0° to 70°. The integration of EQE at 0° incident angle over solar spectrum gives a  $J_{sc}$  of 18.9 mA/cm<sup>2</sup> which is consistent with the value read from photocurrent-voltage measurement. The  $J_{sc}$  at 10° to 50° can still be over 18.3 mA/cm<sup>2</sup>, but drops slightly at higher angles of 60° and 70° due to the strong light reflection/scattering. This result implies that perovskite solar cell is promising for building integrated photovoltaics (BIPV) considering its good performance under a broad range of light incident angle with respect to the sun without relying on a complex solar tracking system. The steady photocurrent measured at the maximum power point of 0.732 V is shown in Figure 4d. The photocurrent increased immediately to a steady value of 16.7 mA/cm<sup>2</sup> under one sun light, giving a stabilized PCE of 12.2%. Thus the colorful device based on the photonic structured OTP layer keeps 80% PCE of the optimized black OTP device fabricated in a similar way which has a PCE of 15.1%<sup>25</sup>. This result indicates that very complexly structured

OTP layer can still has high photovoltaic performance, presumably due to OTP layer's superior absorption and carrier transporting properties, and the much less sensitivity to defect related charge recombination.<sup>34</sup>

In conclusion, vivid colorful OTP solar cells have been fabricated by the simple and scalable doctor-blade coating method. The photonic structures on the OTP film responsible for the vivid color appearance form spontaneously by Rayleigh–Bénard convection and the “coffee-ring effect” giving rise to polygon domain pattern and concentric rings in each domain with near equal ring spacing. By tuning the temperature and precursor solution concentration, the domain size can be continuously tuned from 20  $\mu\text{m}$  to 100  $\mu\text{m}$ , and the ring spacing can be tuned from 2  $\mu\text{m}$  to 6  $\mu\text{m}$ , providing the ability to fine tune the photonic structure periodicity in a convenient way. This scalable, non-lithographic fabrication of photonic structured OTP film without significantly sacrificing its superior optoelectronic performance shall open up a new application for OTP material based optoelectronic device. It should be noted that this photonic structure may be reproducible in other solution processable solar cells with similar approach, as the principle is general fluid dynamics. Nevertheless, the device efficiency of other types of colorful solar cells might be much higher lower. We speculate this photonic structure is uniquely applicable in OTP solar cells. This is because the relative large layer thickness needed to form the photonic structure generally cause severe device performance degradation in many other semiconductor photovoltaic devices. The unusual defect physics in the OTP materials of tolerant to defects enables relative high efficiency device with such photonics structures, despite there is still minor reduction of device efficiency. Future study can further increase the device efficiency by maintaining the photonic structure while significantly reducing the grain boundaries because grain boundaries are shown to be charge recombination sites in OTP solar cells.<sup>33</sup> A

semitransparent and colorful OTP solar cell is also possible based on this method because of the presence of plenty of ring to ring gaps on the photonic structured active layer that light can pass through.

## Materials and Methods

**Colorful perovskite solar cell fabrication.** Indium tin oxide (ITO) coated glass substrates were cleaned with acetone, detergent, deionized water, and isopropanol successively. Before spin-coating, the substrates were treated by UV-ozone cleaner (Jelight 42) for 15 min. PTAA in 1,2-dichlorobenzene (DCB) (5 mg/ml) was spin-coated onto the ITO substrates at 6000 rpm for 30 s and annealed in nitrogen atmosphere at 100 °C for 10 min. Then, the PTAA covered ITO substrates were treated by Argon plasma for 15 second and used immediately.

Methylammonium iodide ( $\text{CH}_3\text{NH}_3\text{I}$ , MAI) and  $\text{PbI}_2$  dissolved in dimethylformamide (DMF) in 1:1 molar ratio were used as doctor blade coating precursor solution. The overall concentration is from 140 mg/ml to 540 mg/ml. The solution ( $\sim 16 \mu\text{l}$ ) was dropped onto PTAA-covered ITO substrate on a hotplate with temperature from 100 °C to 160 °C, and swiped linearly by a glass blade at a speed of 0.75 cm/s. The as-deposited perovskite films were then annealed at 100 °C for 60 minutes. It should be noted that the critical difference between preparing black perovskite films and colorful films is the concentration of precursor solution. As is shown in supporting information Fig. S1, when the concentration of the precursor is high (e. g. 540 mg/ml), there is no concentric ring structure in the final perovskite film, which is not colorful accordingly. When the concentration is decreased to below 350 mg/ml, concentric ring structure appears, and the perovskite films become colorful. After that, 20 mg/ml  $\text{PC}_{60}\text{BM}/\text{DCB}$

solution was spin-coated on top of the perovskite layer at 6000 rpm for 35 s, and the films were further thermally annealed at 100 °C for 60 minutes. All of the above experiments were conducted in N<sub>2</sub> glove box. Finally, C<sub>60</sub> (20 nm), BCP (8 nm) and Al electrode (100 nm) were deposited by thermal evaporation sequentially.

**Solar cell performance characterization.** The solar cells' current-voltage (IV) curves and steady photocurrent under bias were measured with a source-meter (Keithley 2400) under simulated AM 1.5G irradiation by a Xenon lamp (Oriel 67005). External quantum efficiency (EQE) was obtained with a Newport QE measurement kit. Top view and cross-section SEM was performed with Quanta 200 FEG ESEM.

### **Acknowledgement**

We thank the financial support from Office of Naval Research (GRANT11903095) and National Science Foundation (Award ECCS-1252623).

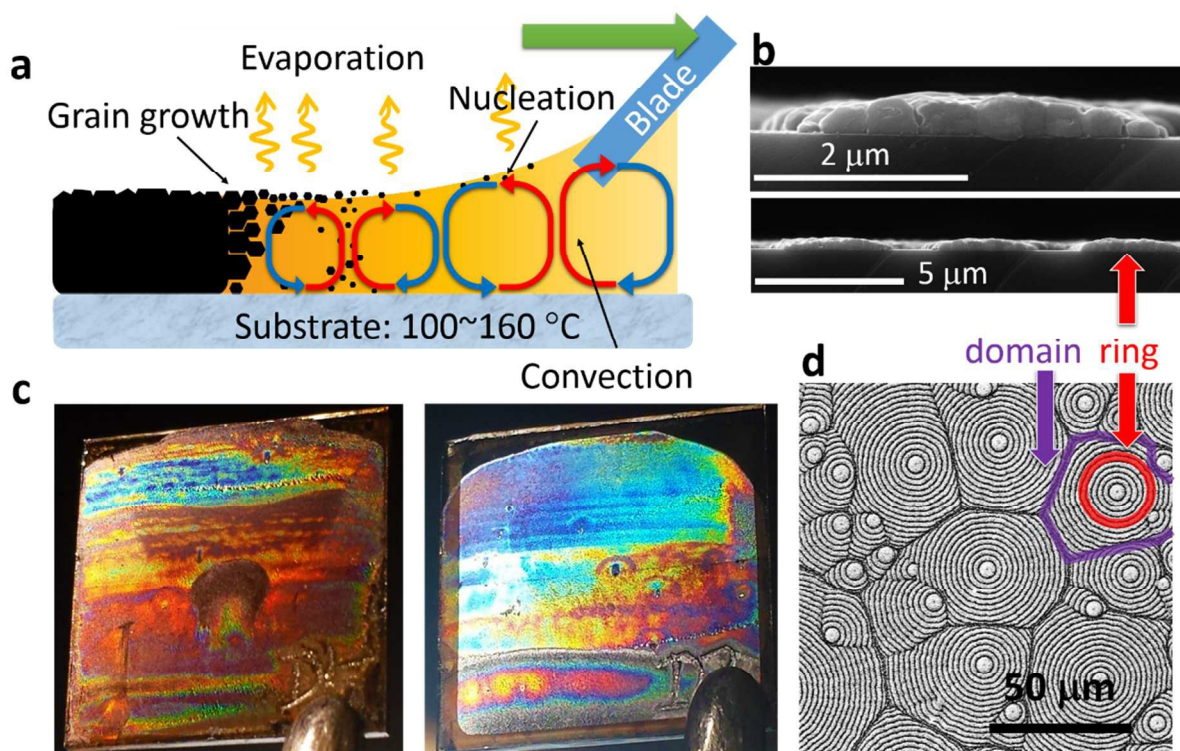


**Figure 1.** (a) An illustration for doctor blade coating of organometal trihalide perovskite (OTP) films on a preheated substrate. (b) Cross section SEM of concentric ring structure in an as-prepared colorful OTP film. (c) Photograph of the as-prepared colorful OTP film and complete device with aluminum electrode on top. Both samples were placed under 1 sun simulated illumination. (d) Plane view SEM of the as-prepared colorful OTP film showing polygon domains and concentric ring structure in each domain.

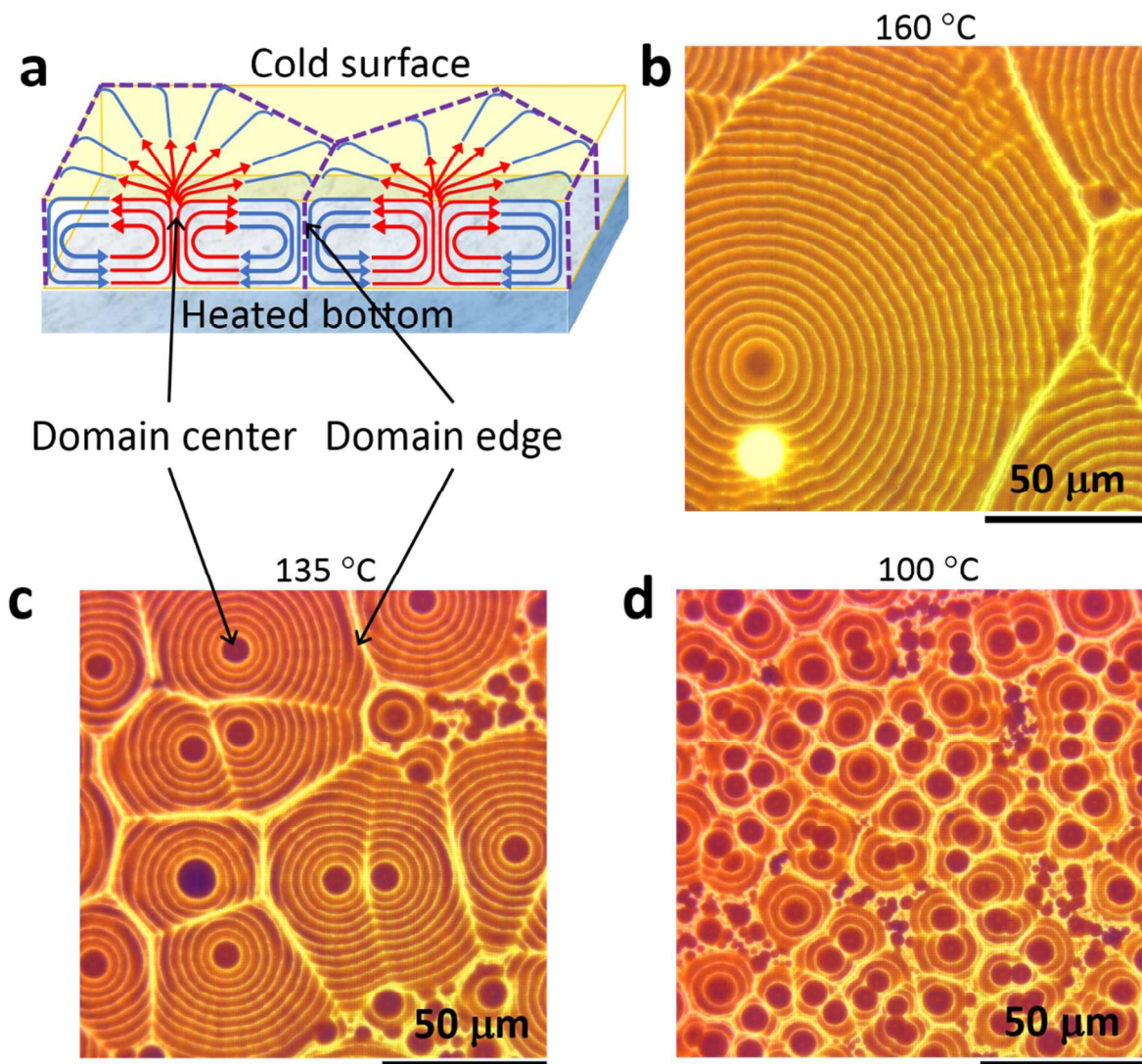


**Figure 2.** (a) An illustration for Rayleigh–Bénard convection cell in a thin solution film driven by temperature difference between heated bottom and cold top surface. (b)–(d) Microscopic image of as-prepared colorful OTP films prepared when the substrate temperature is at 160 °C, 135 °C, and 100 °C, respectively.

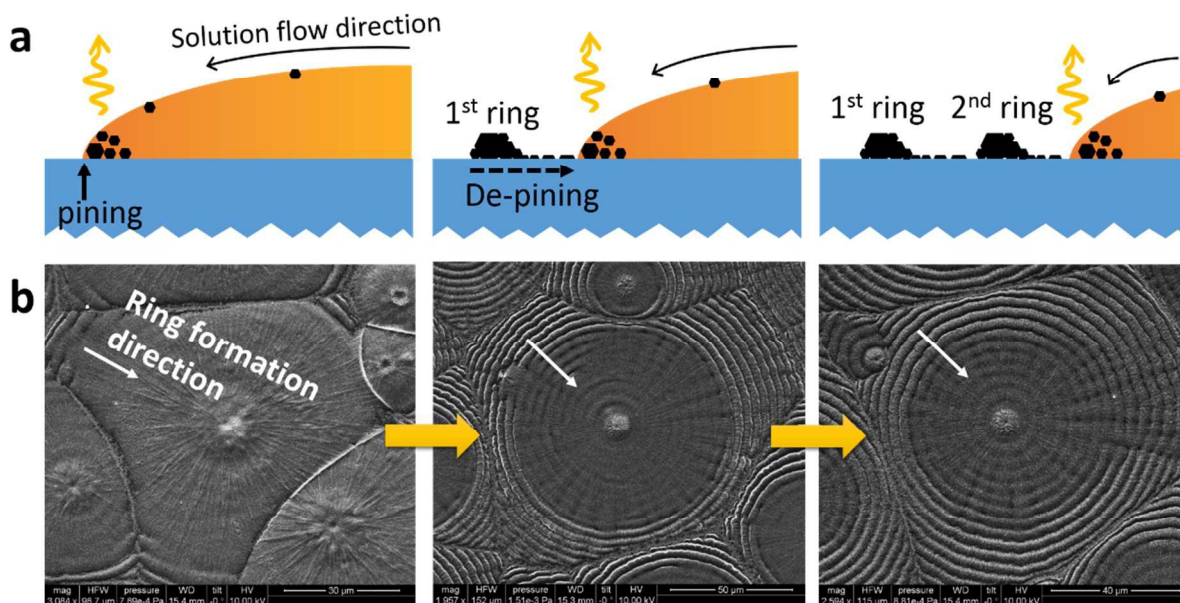


**Figure 3.** (a) An illustration for concentric ring structure formation from “coffee ring” effect with the contact line contracts in a manner of pinning/de-pinning process. (b) SEM images of concentric ring structures formation at different stages “frozen” by dropping a droplet of toluene onto the wet film during drying.

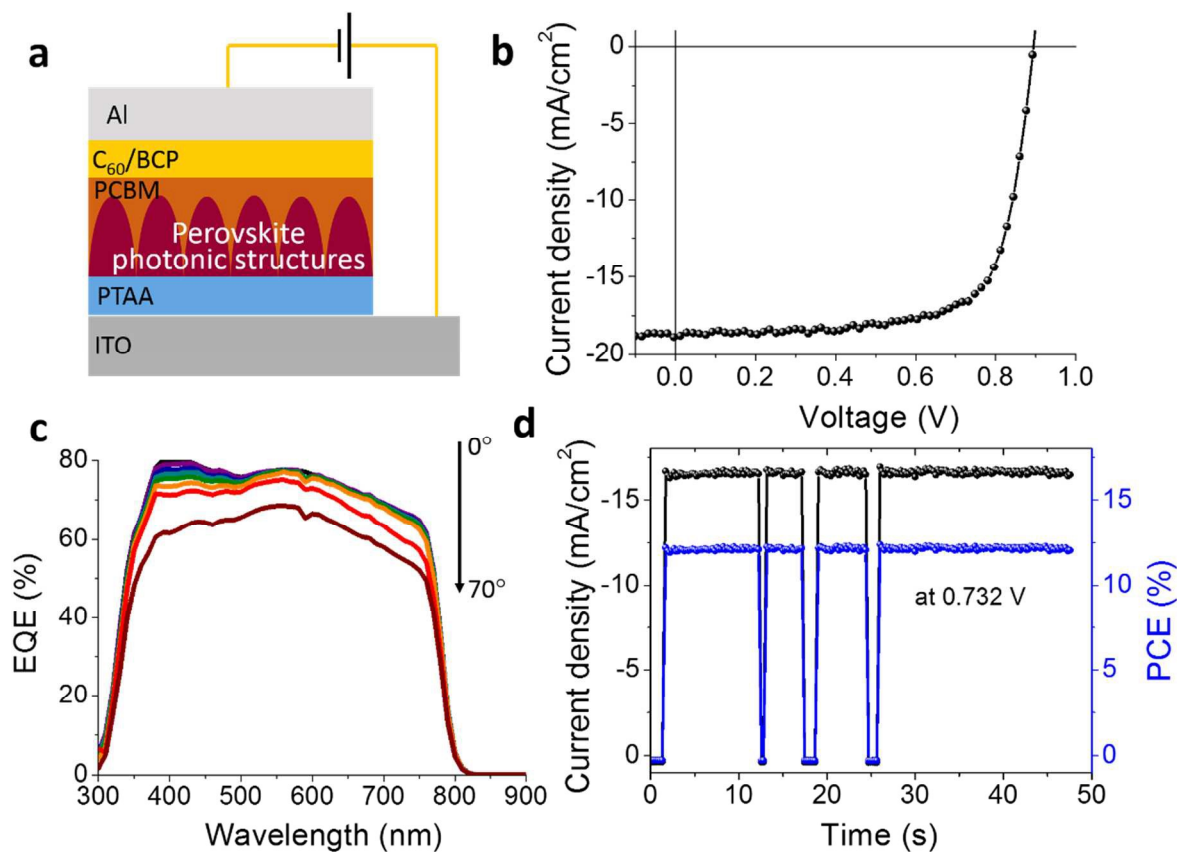


**Figure 4.** (a) An illustration for colorful OTP solar cell device structure. (b) Photocurrent-voltage scanning of the solar cell under one sun illumination ( $100 \text{ mW}/\text{cm}^2$ ). (c) External quantum efficiency (EQE) of the colorful OTP solar cells measured at different angle between the incident light and the normal direction of the solar cell plane. (d) Stabilized photocurrent measured at the maximum power point (0.732 V) and the PCE.

## References

1. A. Henemann, *Renewable Energy Focus*, 2008, **9**, 14-19.
2. B. Petter Jelle, C. Breivik and H. Drolsum Røkenes, *Solar Energy Materials and Solar Cells*, 2012, **100**, 69-96.
3. M. B. Schubert and J. H. Werner, *Materials Today*, 2006, **9**, 42-50.
4. K. S. Chen, J. F. Salinas, H. L. Yip, L. Huo, J. Hou and A. K. Y. Jen, *Energy & Environmental Science*, 2012, **5**, 9551.
5. H. Park, T. Xu, J. Lee, A. Ledbetter and L. Guo, *ACS Nano*, 2011, **5**, 7055-7060.
6. W. Yu, X. Jia, Y. Long, L. Shen, Y. Liu, W. Guo and S. Ruan, *ACS applied materials & interfaces*, 2015, **7**, 9920-9928.
7. J. Y. Lee, K. T. Lee, S. Seo and L. J. Guo, *Scientific reports*, 2014, **4**, 4192.
8. K. T. Lee, J. Y. Lee, S. Seo and L. J. Guo, *Light: Science & Applications*, 2014, **3**, e215.
9. K. T. Lee, M. Fukuda, S. Joglekar and L. J. Guo, *J. Mater. Chem. C*, 2015, **3**, 5377-5382.
10. U. W. Paetzold, W. Qiu, F. Finger, J. Poortmans and D. Cheyns, *Applied Physics Letters*, 2015, **106**, 173101.
11. W. Zhang, M. Anaya, G. Lozano, M. E. Calvo, M. B. Johnston, H. Miguez and H. J. Snaith, *Nano letters*, 2015, **15**, 1698-1702.
12. M. A. Kats, R. Blanchard, P. Genevet and F. Capasso, *Nature materials*, 2013, **12**, 20-24.
13. K. Diest, J. Dionne, M. Spain and H. Atwater, *Nano letters*, 2009, **9**, 2579-2583.
14. B. E., W. Pesch and G. Ahlers, *Annual review of fluid mechanics*, 2000, **32**, 709-778.
15. M. Golubitsky, J. W. Swift and E. Knobloch, *Physica D: Nonlinear Phenomena*, 1984, **10**, 249-276.
16. T. Hartlep, A. Tilgner and F. H. Busse, *Physical Review Letters*, 2003, **91**, 064501.

17. D. C. Rapaport, *Physical Review E*, 2006, **73**.
18. A. V. Getling, *Soviet Physics Uspekhi*, 1991, **34**, 737-776.
19. R. D. Deegan, O. Bakajin, T. F. Dupont, G. Huber, S. R. Nagel and T. A. Witten, *Nature*, 1997, **389**, 827-829.
20. E. Adachi, A. S. Dimitrov and K. Nagayama, *Langmuir*, 1995, **11**, 1057-1060.
21. M. E. Shanahan, *Langmuir*, 1995, **11**, 1041-1043.
22. S. W. Hong, J. Xu, J. Xia, Z. Lin, F. Qiu and Y. Yang, *Chemistry of materials*, 2005, **17**, 6223-6226.
23. P. J. Yunker, T. Still, M. A. Lohr and A. G. Yodh, *Nature*, 2011, **476**, 308-311.
24. W. Han and Z. Lin, *Angewandte Chemie*, 2012, **51**, 1534-1546.
25. Y. Deng, E. Peng, Y. Shao, Z. Xiao, Q. Dong and J. Huang, *Energy & Environmental Science*, 2015, **8**, 1544-1550.
26. W. Nie, H. Tsai, R. Asadpour, J. C. Blancon, A. J. Neukirch, G. Gupta, J. Crochet, M. Chhowalla, S. Tretiak, M. A. Alam, H. Wang and A. D. Mohite, *Science*, 2015, **347**, 522-525.
27. M. Xiao, F. Huang, W. Huang, Y. Dkhissi, Y. Zhu, J. Etheridge, A. Gray-Weale, U. Bach, Y. B. Cheng and L. Spiccia, *Angewandte Chemie International Edition*, 2014, **126**, 10056-10061.
28. N. J. Jeon, J. H. Noh, Y. C. Kim, W. S. Yang, S. Ryu and S. I. Seok, *Nature materials*, 2014, **13**, 897-903.
29. C. Bi, Q. Wang, Y. Shao, Y. Yuan, X. Z. and J. Huang, *Nature Communications* (*accepted*), 2015.
30. Q. Wang, C. Bi and J. Huang, *Nano Energy*, 2015, **15**, 275-280.

31. Q. Wang, Y. Shao, Q. Dong, Z. Xiao, Y. Yuan and J. Huang, *Energy & Environmental Science*, 2014, **7**, 2359-2365.
32. Z. Xiao, C. Bi, Y. Shao, Q. Dong, Q. Wang, Y. Yuan, C. Wang, Y. Gao and J. Huang, *Energy & Environmental Science*, 2014, **7**, 2619-2623.
33. S. M. Vorpahl, S. D. Stranks, H. Nagaoka, G. E. Eperon, M. E. Ziffer, H. J. Snaith and D. S. Ginger, *Science*, 2015, **348**, 683-686.
34. W. J. Yin, T. Shi and Y. Yan, *Advanced materials*, 2014, **26**, 4653-4658.